J Mater Sci

Energy materials

CaO impregnated highly porous honeycomb activated carbon from agriculture waste: symmetrical supercapacitor study

Gomaa A. M. Ali[1,2,3,*], Omar Abed Habeeb[4], H. Algarni[5,6], and Kwok Feng Chong[1,*]

[1] *Faculty of Industrial Sciences and Technology, Universiti Malaysia Pahang, 26300 Gambang, Kuantan, Malaysia*
[2] *Chemistry Department, Faculty of Science, Al–Azhar University, Assiut 71524, Egypt*
[3] *Al–Azhar Center of Nanoscience and Applications (ACNA), Al–Azhar University, Assiut 71524, Egypt*
[4] *Faculty of Chemical and Natural Resources Engineering, Universiti Malaysia Pahang, 26300 Gambang, Kuantan, Malaysia*
[5] *Research Centre for Advanced Materials Science (RCAMS), King Khalid University, P. O. Box 9004, Abha 61413, Saudi Arabia*
[6] *Department of Physics, Faculty of Sciences, King Khalid University, P. O. Box 9004, Abha 61413, Saudi Arabia*

Received: 20 June 2018
Accepted: 28 August 2018

ABSTRACT

This study presents the electrochemical studies of activated carbon prepared from palm kernel shell (ACPKS), with CaO impregnation. The CaO is obtained from chicken eggshell waste to produce CaO/ACPKS, which shows highly porous honeycomb structure with homogeneous distribution of CaO nanoparticles (30–50 nm in size). The prepared materials are evaluated as supercapacitor electrodes by testing their electrochemical characteristics. A high specific capacitance value of 222 F g^{-1} at 0.025 A g^{-1} is obtained for CaO/ACPKS, which is around three times higher than that for ACPKS (76 F g^{-1}). In addition, electrochemical impedance data show lower impedance for CaO/ACPKS. Lastly, a practical symmetrical supercapacitor is fabricated by CaO/ACPKS and its performance is discussed.

Introduction

As a move to preserve the environment with low-cost material, waste precursors can be the potential source for the production of carbon-based materials. Oil palm biomass residues (leaves, fronds, trunks, fruit bunches, kernel shells and fibers), produced from oil palm industries, are abundant in southeast Asia [1], with around 73.74 million tons per year in Malaysia [2]. A common practice in managing oil palm residues is burning, which gives rise to environmental issues. Furthermore, it is a loss from the economic point of view as these wastes are composed of high carbon content (about 18 wt%) [2] and can be the potential source for the production of carbon-based material.

Carbon materials have a crucial role in the fabrication and development of alternative clean and sustainable energy technologies (supercapacitor

Address correspondence to E-mail: gomaasanad@azhar.edu.eg; ckfeng@ump.edu.my

https://doi.org/10.1007/s10853-018-2871-6

Published online: 05 September 2018

electrode construction) [3–6]. Many carbon-based materials are widely studied for energy storage supercapacitor due to their abundance, high surface area, good electrical conductivity, low production cost, high power and energy densities, short charging time and long cycling stability. These carbon materials include activated carbon (AC), C60, carbon nanotubes in both forms single-walled (SWCNTs) and multi-walled (MWCNTs), single-walled carbon nanohorns (SWCNHs), carbon nanospheres, carbon nanoparticles, carbon nano-onions, carbon capsules and graphene [7–15].

Carbon materials have been synthesized from different waste sources such as banana fibers, argan (Argania spinosa) seed shells, corn grains, camellia oleifera shell, oil palm (empty fruit bunches and leaves), sugarcane bagasse and scrap waste tires [8, 16–19]. AC prepared from camellia oleifera shell showed a specific capacitance of 374 and 266 F g^{-1} in 1 M H_2SO_4 and 6 M KOH electrolytes, respectively [8]. In addition, the symmetrical supercapacitor by the activated carbon from sugar cane bagasse exhibited a specific energy and capacitance of 10 Wh kg^{-1} and 300 F g^{-1}, respectively [16]. The electrochemical behavior of the carbon material derived from banana fibers chemically activated by KOH and $ZnCl_2$ was studied in a neutral electrolyte (1 M Na_2SO_4), the non-faradaic electrostatic sorption of ions at the electrode surface mainly governs the electrode capacitance [3, 17].

In addition, CaO could be obtained from eggshell as waste precursor [20, 21]. CaO impregnated AC was used as a catalyst for the deoxygenation in biodiesel production [20, 22]. To the best of our knowledge, calcium-based AC has not been reported as a supercapacitor electrode. The incorporation of calcium was found to enhance the charge storage ability, the electrical conductivity and the electrochemically active surface area [23]. This study aims to investigate and evaluate the low-cost electrode materials for supercapacitor application. The materials in this work were prepared from palm kernel shell and they were impregnated with CaO from waste eggshell. Their morphological and surface area properties were studied as they play a critical role for the ions adsorption as well as diffusion during electrochemical process. Detailed electrochemical studies were conducted on a single electrode and practical symmetrical supercapacitor, using cyclic voltammetry (CV), galvanostatic charge–discharge (CDC) and electrochemical impedance spectroscopy (EIS).

Materials and methods

Samples preparation and characterization

The activated carbon was prepared from palm kernel shells and termed as ACPKS. The prepared ACPKS was then impregnated with CaO obtained from chicken eggshell waste and termed as CaO/ACPKS. The sample preparation and characterization were reported in detail in our previous works [21, 24]. Briefly, palm kernel shells waste was provided by United Palm Oil Mill, Nibong Tebal, Malaysia, washed with deionized water, dried at 105°C and then followed by mechanical grinding. The sample (0.5–1.0 mm) was mixed with KOH (1:4) and heated in a tubular horizontal furnace at 750°C for 2 h in N_2 atmosphere to perform carbonization process. The produced AC was cooled and washed with diluted HCl and deionized water. On the other hand, the chicken eggshells waste (CaO precursor) was collected, cleaned from impurities, blended, sieved (0.25–0.5 mm) and finally dried at 105°C. The obtained material was soaked in acetic acid to get a calcium solution. Finally, this calcium solution was utilized for the AC impregnation. A ratio of 0.2 g of AC per mL of calcium solution was utilized. All experiments were performed at 30°C using a temperature-controlled stirrer operated at 150 rpm and the contact time of 4 h. Finally, the impregnated AC was heated at 800°C for 1.5 h to obtain CaO/ACPKS. As the electrochemical properties are directly dependent on the materials morphology and composition, therefore their surface morphology was monitored by a JEOL (JSM7800F) field emission scanning electron microscope (FESEM) connected with EDX mapping.

Electrochemical studies

The electrodes were fabricated from the active materials (CaO/ACPKS and ACPKS), carbon black and polyvinylidene fluoride in the weight ratio of 90:5:5 on nickel foam. The active material mass on the electrode was around 5 mg. The electrochemical performance was studied using three-electrode system which consists of the active material, Ag/AgCl

(CH Instrument) and Pt wire (CH Instrument) as working, reference and counter electrodes, respectively. A practical symmetrical supercapacitor was made using two electrodes with active material sandwiched and pressed into a coin cell design. The electrochemical data were collected using potentiostat/galvanostat equipped with frequency response analyzer (AUTOLAB PGSTAT30). CV tests were performed in different potential ranges at different scan rates. CDC tests were performed at different current densities. EIS data were collected from 50 kHz to 0.01 Hz, at open circuit potential (OCP) with a.c. amplitude of 10 mV. 1 M Na_2SO_4 was used as electrolyte throughout all electrochemical measurements.

Results and discussion

Structural and morphological analyses

Detailed analyses of samples were reported in our previous works [21, 24]. FESEM images show highly porous honeycomb structure of both ACPKS and CaO/ACPKS (see Fig. 1). For CaO/ACPKS, CaO nanoparticles in the size range of 30 to 50 nm are homogeneously distributed on the surface of AC. The elemental analyses were performed by EDX as shown in Fig. S1 and listed in Table S1. For ACPKS, high carbon (80.15%) and low oxygen (18.19%) contents are shown together with very low amount of potassium (1.66%) which may be attributed to the KOH used for the activation process. On the other hand, CaO/ACPKS shows 6.39% calcium as a result of the successful impregnation process as confirmed by FESEM images. In addition, surface area analyses showed the high surface area of 776.4 and 476.7 $m^2\ g^{-1}$ for ACPKS and CaO/ACPKS, respectively (see Fig. 2). The lower surface area for CaO/ACPKS could be associated with the pores blockage by CaO particles [25]. Nonetheless, both ACPKS and CaO/ACPKS demonstrated the comparable mesoporosity with average pore diameters of 3.9 and 3.5 nm for ACPKS and CaO/ACPKS, respectively. Consequently, the void fraction is found to be 43% for ACPKS and 28% for CaO/ACPKS. This mesoporosity is crucial for ions adsorption and diffusion during the electrochemical process and its effect toward charge storage is further investigated in this work.

Electrochemical studies

Electrochemical performance of the supercapacitor electrode

In order to confirm the potential limit of ACPKS electrode, CV and CDC were performed in 1 M Na_2SO_4 in different potential windows as shown in Fig. S2a-b at 25 mV s^{-1} and 1 A g^{-1}, respectively. The curve is clear rectangular voltammogram in the potential range from − 0.4 to 0.6 V with the highest Coulombic efficiency of 98.3%. In addition, CDC shows a linear curve with the highest Coulombic efficiency of 98.9% in the same potential window (− 0.4 to 0.6 V). Other potential ranges show the redox activity of the electrolyte and the deviation from CDC linearity. Therefore, the subsequent electrochemical tests were conducted in the potential range of − 0.4 to 0.6 V.

Figure 3a, b shows CV curves for ACPKS and CaO/ACPKS electrodes at different scan rates, respectively. Both electrodes exhibit rectangular-like shapes without any faradaic redox peaks at all scan rates. This reveals the ideal electrochemical double layer capacitance (EDLC) behavior for both electrodes and the absence of pseudocapacitance effect.

The charge storage mechanism in ACPKS and CaO/ACPKS electrodes were investigated by Trasatti's analysis, according to the following equations [26, 27]:

$$Q_{(\upsilon)} = Q_C + \alpha\upsilon^{-1/2} \quad (1)$$

$$1/Q_{(\upsilon)} = 1/Q_T + \alpha\upsilon^{1/2} \quad (2)$$

where $Q_{(\upsilon)}$ and Q_C are the total measured the voltammetric charge and capacitive charge, respectively, Q_T is the total amount of stored charge, α is a constant and υ represents the scan rate. Q_C can be obtained by extrapolating the plot of $Q_{(\upsilon)}$ versus $\upsilon^{-1/2}$ (Fig. 3c); while Q_T can be obtained by extrapolating the plot of $1/Q_{(\upsilon)}$ versus $\upsilon^{1/2}$ (Fig. 3d). Diffusive charge (Q_D) which is associated with the ions intercalation and it can be obtained from the difference between Q_T and Q_C. The summary of Q_D, Q_C and Q_T values is tabulated as Table 1. As expected, ACPKS exhibits high EDLC behavior by having dominant charge storage in the capacitive mode (Q_C of 76.3%). It is worth mentioning that the impregnation of CaO in the CaO/ACPKS changes the charge storage behavior into the diffusive mode (Q_D of 75.2%). It

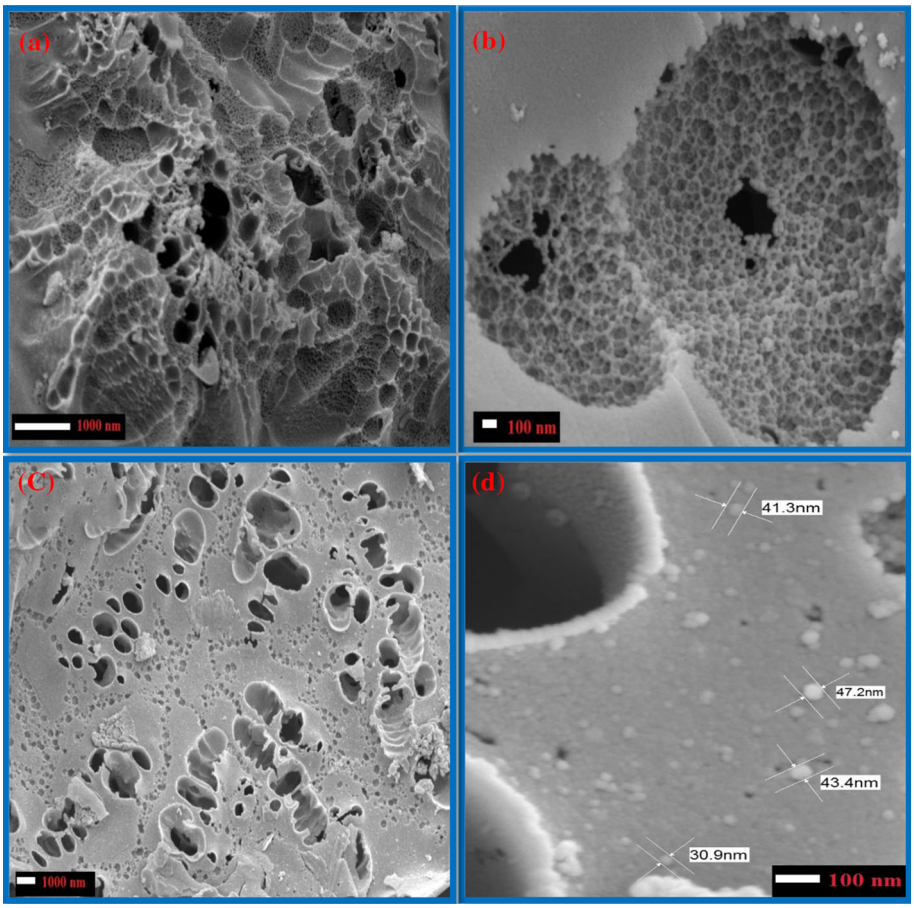

Figure 1 FESEM images of **a**, **b** ACPKS and **c**, **d** CaO/ACPKS.

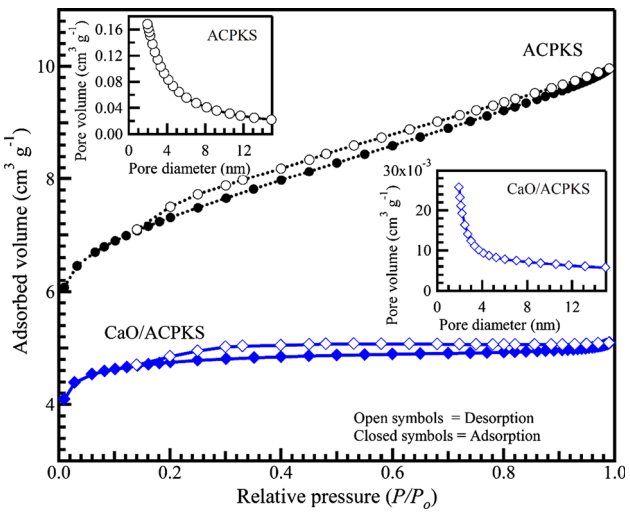

Figure 2 N_2 adsorption–desorption isotherms of ACPKS and CaO/ACPKS: the insets show the pore size distributions.

implies that more charges are stored through the intercalation/de-intercalation of ions on the CaO/ACPKS structure. Nanometer pore diameter is proven to facilitate ions adsorption in supercapacitors [28, 29]. On the other hand, CDC curves of both electrodes at different current densities are shown in Fig. 4a, b. Both electrodes show a similar trend by having linear curves under a wide range of current, with negligible *iR* drop (4.3 mV which is around 0.71% of the total potential window) as shown in the insets of Fig. 4a, b. Basically, *iR* drop (in terms of energy) is the energy dissipated during the flow of electrons due to any kind of resistance in the device. Figure 4c compares CDC curves at 0.25 A g^{-1} for ACPKS and CaO/ACPKS and clearly shows the longer discharge time of CaO/ACPKS as compared to ACPKS, indicating higher charge accumulation and higher capacitance. The specific capacitance was obtained from CDC data using the equation reported elsewhere [21, 30]. Figure 4d shows the specific capacitance for ACPKS and CaO/ACPKS as a function of current density. CaO/ACPKS shows high specific capacitance value of 222 F g^{-1} at 0.025 A g^{-1}, which is around 3-times higher than that for ACPKS (76 F g^{-1} at 0.025 A g^{-1}). As revealed by Trassati's analysis, the capacitance enhancement in CaO/

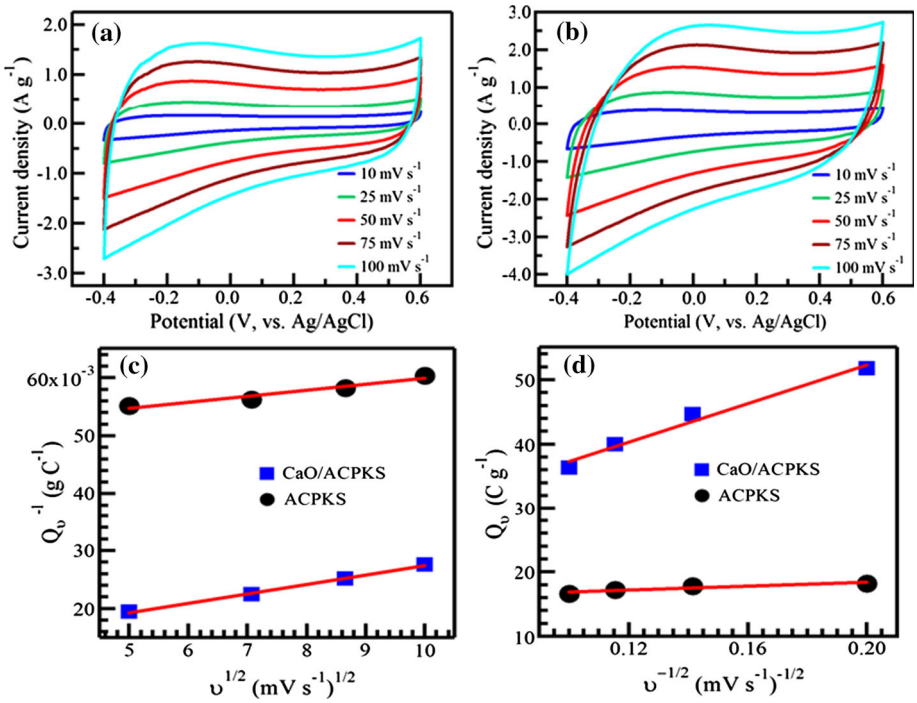

Figure 3 Cyclic voltammetry curves at different scan rates for **a** ACPKS and **b** CaO/ACPKS; Dependence of **c** $Q_{(\upsilon)}$ on $\upsilon^{-1/2}$ and **d** $1/Q_{(\upsilon)}$ on $\upsilon^{1/2}$ for ACPKS and CaO/ACPKS.

Table 1 Total charge (Q_T), capacitive charge (Q_C), diffusive charge (Q_D) and the ratios Q_C/Q_T and Q_D/Q_T for ACPKS and CaO/ACPKS

Electrodes	Q_T (C g^{-1})	Q_C (C g^{-1})	Q_D (C g^{-1})	Q_C/Q_T (%)	Q_D/Q_T (%)
ACPKS	20.2	15.4	4.8	76.3	23.7
CaO/ACPKS	90.1	22.3	67.8	24.8	75.2

ACPKS can be attributed to the intercalation/de-intercalation of ions on CaO/ACPKS, as compared to the pure EDLC of ACPKS. These findings are also compared with specific capacitance values of AC impregnated with other materials, including carbon, polymer and metal oxide as listed in Table 2.

Figure 5 shows Nyquist plots obtained in 1 M Na_2SO_4 at OCP for both for ACPKS and CaO/ACPKS electrodes. The insets are the high-frequency region zoomed view of measured and the equivalent circuit used for data fitting. The Nyquist plots show a semicircle in the high-frequency region and a near-vertical line at low frequency. The near-vertical line in the low-frequency region indicates the good capacitive of the cell. The solution resistance (R_s) values were estimated from the intercept at the real axis of the high-frequency range and charge transfer resistance (R_{ct}) values were estimated from the diameter of the semicircle. Solution resistance (R_s) values were found to be 2.62 and 0.92 Ω for ACPKS and CaO/ACPKS electrodes, respectively. The charge transfer resistance (R_{ct}) values were found to be 0.86 and 0.44 Ω for ACPKS and CaO/ACPKS electrodes, respectively. CaO/ACPKS shows very low resistances if compared to reduced graphene oxide (0.58 Ω) [50], $RuO_2{\cdot}xH_2O$/carbon nano-onions (0.585 Ω) [11], oil palm fronds (0.62 Ω) [7] and MWCNTs (5.13 Ω) [51]. In addition, the capacitance, constant phase element and Warburg resistance were found to be (0.25 mF, 0.037 Ω^{-1} s^n and 0.08 Ω) and (0.37 mF, 0.013 Ω^{-1} s^n and 0.13 Ω) for ACPKS and CaO/ACPKS electrodes, respectively. The smaller impedance on CaO/ACPKS indicates the CaO impregnation could improve the structural conductivity. The electrochemical active specific surface area (S_E) can be estimated from Eq. (3) as [30]:

$$S_E = \frac{C_{dl}}{C_d} \tag{3}$$

where C_d is the areal capacitance for carbon material (20 μF cm^{-2}); C_{dl} was obtained from EIS data at 0.01 Hz using the equation: $C_{dl} = 1/(2\pi fmZ'')$ [52], where, f is the frequency and Z'' is the impedance imaginary part. The calculated values of S_E at OCP

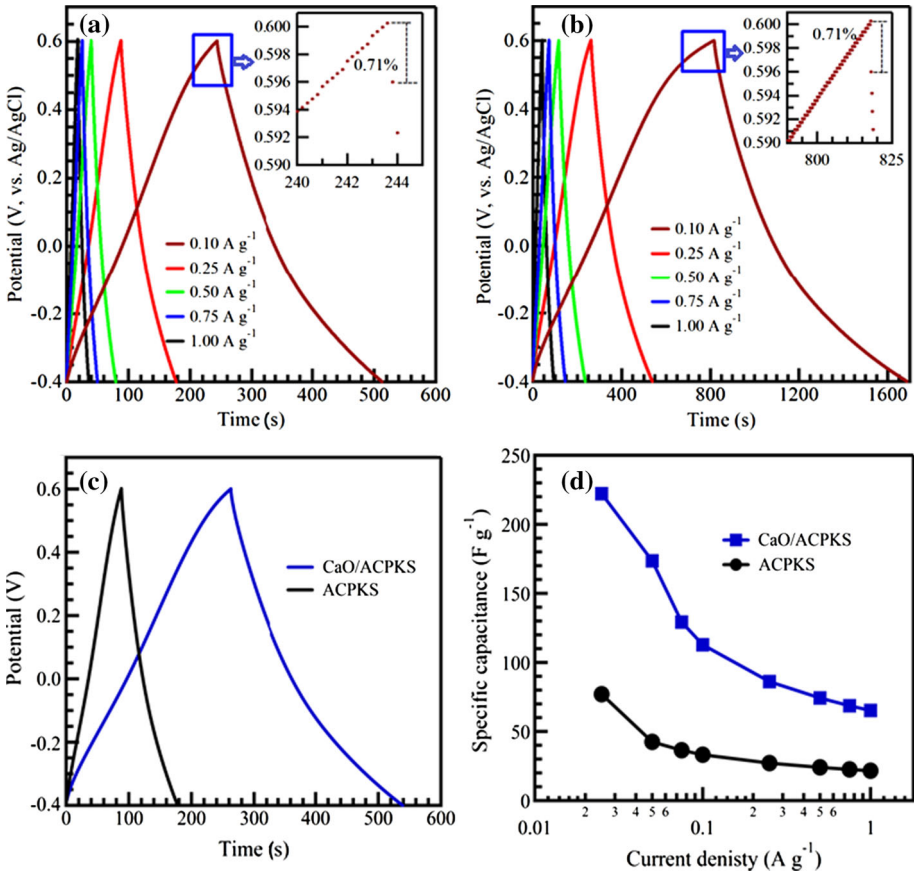

Figure 4 Charge–discharge curves at different current densities for **a** ACPKS, **b** CaO/ACPKS, **c** at 0.25 A g^{-1} and **d** specific capacitance as a function of current density for both electrodes: insets show high magnification areas to display the *iR* drop.

Table 2 Specific capacitance comparison with impregnated carbon-based materials

Type	Electrode materials	Specific capacitance (F g^{-1})	References
Carbon/AC	CNT/AC	165 @ 0.1 A g^{-1}	[31]
	Fullerene (C_{60})/AC	170 @ mA cm^{-2}	[10]
	Graphene/AC	273 @ 0.5 A g^{-1}	[32]
Polymer/AC	Polyethylenedioxythiophene/AC	158 @ 10 mV s^{-1}	[33]
	Polyaniline/AC	159.37 @ 2.5 mA cm^{-2}	[34]
	Polyaniline/AC	338.15 @ 1 A g^{-1}	[35]
	Polypyrrole/AC	530 @ 2 mV s^{-1}	[36]
Metal oxide/AC	MnO_2/AC	50.6 @ 0.1 A g^{-1}	[37]
	MnO_2/AC	60 @ 0.1 A g^{-1}	[38]
	Cu/AC	78.9 @ 0.2 A g^{-1}	[39]
	$Li_4Ti_5O_{12}$/AC	83 @ 0.06 A g^{-1}	[40]
	TiO_2/AC	92 @ 5 mV s^{-1}	[41]
	NiO/AC	107 @ 5 mV s^{-1}	[25]
	ZnO/AC	160 @ 2 mV s^{-1}	[42]
	ZnO/AC nanofiber	178.2 @ 1 mA cm^{-2}	[43]
	MoO_3-carbon nanocomposite	179 @ 0.05 A g^{-1}	[44]
	NiO/AC	196.71 @ 10 mA cm^{-2}	[45]
	MnO_2/activated mesocarbon	228 @ 10 mV s^{-1}	[46]
	Fe_2O_3/AC	240 @ 1 A g^{-1}	[47]
	RuO_2/AC	256 @ 0.1 A g^{-1}	[48]
	MnO_2/AC	271.5 @ 10 mV s^{-1}	[49]
	CaO/*ACPKS*	222 @ 0.025 A g^{-1}	*This work*

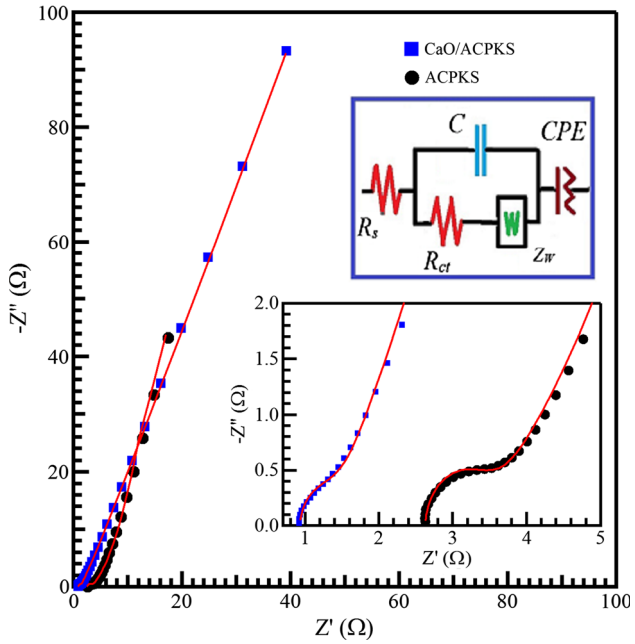

Figure 5 Nyquist plots for ACPKS and CaO/ACPKS, the insets show the equivalent circuit and high-frequency region magnification: The solid lines are the fitting results.

were found to be 144.9 and 57.6 $m^2\ g^{-1}$ for ACPKS and CaO/ACPKS, respectively.

Electrochemical performance of the practical symmetrical supercapacitor

The energy stored in a supercapacitor is directly proportional to the capacitance and the potential, therefore increasing the operating voltage of supercapacitors is crucial. Generally, the operating voltage is limited by the potential window of the electrolytes [4, 19]. Figure 6a compares the CV curves of symmetrical supercapacitor made by CaO/ACPKS electrodes at 25 mV s^{-1} under potentials windows range from 0.0 to 1.0, 1.2, 1.4, 1.6, 1.8 and 2.0 V. The symmetrical supercapacitor shows the near-rectangular CV shape in all potential windows. The inset of Fig. 6a shows the specific capacitance increases with increasing the potential window. However, CV curves with a potential window of 1.8 and 2.0 V show significant faradaic current at potential higher than 1.8 V, which could be detrimental to its stability. Therefore, the potential window of 1.6 V was used for the subsequent testing. In addition, the CV at all scan rates with potential windows of 1.0 and 1.4 V are shown in Fig. S3a-b. They show near-rectangular CV shape under all scan rates up to 100 mV s^{-1}.

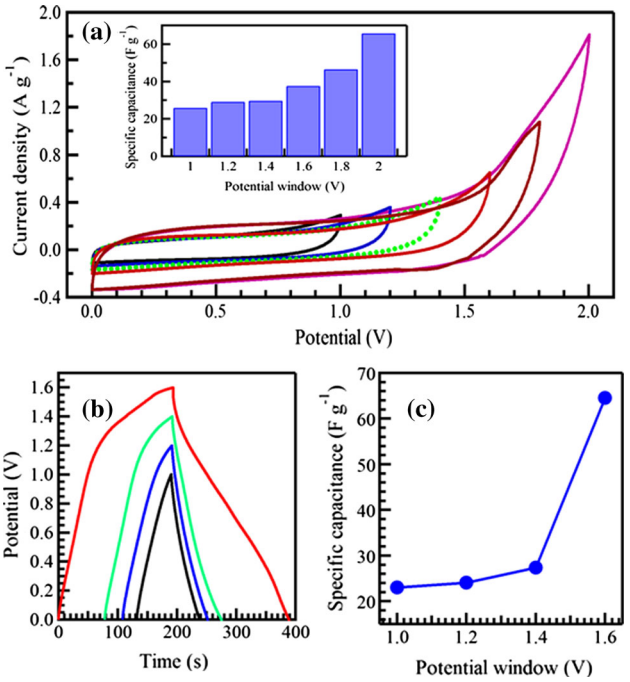

Figure 6 **a** Cyclic voltammetry curves under different potential windows: inset shows the specific capacitance as a function of potential window at 25 mV s^{-1}, **b** charge–discharge curves at 0.1 A g^{-1} under different potential windows and **c** specific capacitance as a function of potential window at 0.1 A g^{-1} for the symmetrical supercapacitor.

Figure 6b shows the linear charge–discharge curves at 0.1 A g^{-1} under different potential ranges. Calculation (Fig. 6c) shows that the highest specific capacitance can be attained at the potential range of 1.6 V. The high capacitance and large operating voltage of this symmetrical supercapacitor implies the high energy storage capability. Moreover, the symmetrical supercapacitor shows a linear discharge curves under different current density range from 0.1 to 1.0 A g^{-1} with potential windows of 1.4 V as shown in Fig. S3c. The specific capacitance is increased with decreasing current density (Fig. S3d).

The symmetrical supercapacitor displays a high potential cycling stability as shown in Fig. 7a. Only about 7% decrease in the specific capacitance is observed after 3300 CDC cycles at 1 A g^{-1}, indicating the repetitive CDC cycling induces noticeable degradation of neither the structure nor the morphology. CV (Fig. 7b) was used to further investigate the electrochemical stability [7, 53]. CV at 25 mV s^{-1} shows identical curves before and after CDC cycling, confirming the high electrochemical stability of CaO/

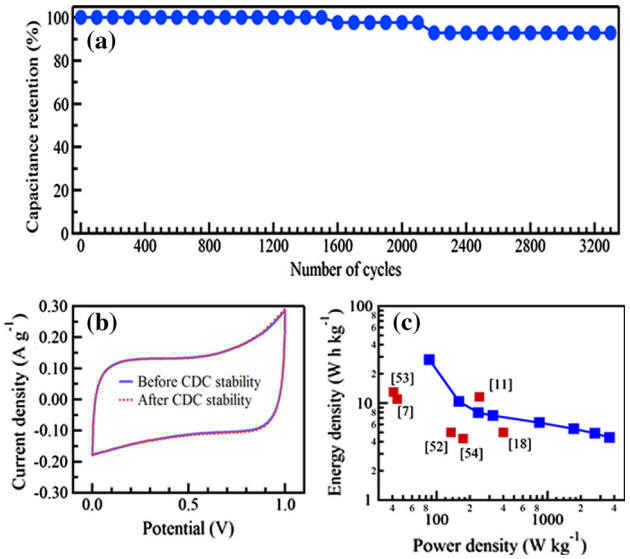

Figure 7 **a** Cycle life stability at 1 A g^{-1} current density, **b** cyclic voltammetry curves at 25 mV s^{-1} before and after charge–discharge stability and **c** Ragone plot of the symmetrical supercapacitor.

ACPKS. Similar behavior was also observed for RuO_2/AC system [48].

The energy (E) and power (P) densities can be calculated from CDC data using Eqs. (4) and (5), respectively [54].

$$E = \frac{1}{2} C_s V^2 \tag{4}$$

$$P = \frac{E}{\Delta t_d} \tag{5}$$

Ragone plot of the practical supercapacitor is shown in Fig. 7c. The supercapacitor shows a high energy density of 27.9 W h kg^{-1} at a power density of 85.7 W kg^{-1}. This energy density is higher than that obtained for porous nanocarbons from biowaste oil palm leaves precursor (13 W h kg^{-1}) [53], $RuO_2{\cdot}xH_2O$/carbon nano-onions (11.6 W h kg^{-1}) [11], oil palm fronds (11 W h kg^{-1}) [7], biowaste sago bark (5 W h kg^{-1}) [18], oil palm empty fruit bunches activated carbon (4.3 W h kg^{-1}) [54] and graphene (5 W h kg^{-1}) [52].

Conclusions

Activated carbon prepared from palm kernel shell and impregnated with CaO from eggshell (CaO/ACPKS) has been investigated as supercapacitor electrodes. CaO/ACPKS shows promising structural and morphological properties supporting their use for energy storage. Cyclic voltammetry and galvanostatic charge–discharge indicate electrochemical double layer capacitance, in addition to the improved ions intercalation/de-intercalation. CaO/ACPKS shows high specific capacitance of 222 F g^{-1} at 0.025 A g^{-1}, which is around 3-times higher than ACPKS. The practical symmetrical supercapacitor of CaO/ACPKS shows high electrochemical stability of 93% and a high energy density of 27.9 W h kg^{-1} at a power density of 85.7 W kg^{-1}.

Acknowledgements

The authors would like to acknowledge the funding from the Ministry of Education Malaysia in the form of FRGS [RDU160118: FRGS/1/2016/STG07/UMP/02/3], Universiti Malaysia Pahang Grant RDU170357 and Deanship of Scientific Research at King Khalid University (R.G.P.2/2/38).

Compliance with ethical standards

Conflict of interest The authors declare that they have no conflict of interest.

Electronic supplementary material: The online version of this article (https://doi.org/10.1007/s10853-018-2871-6) contains supplementary material, which is available to authorized users.

References

[1] Chavalparit O, Rulkens W, Mol A et al (2006) Options for environmental sustainability of the crude palm oil industry in Thailand through enhancement of industrial ecosystems. Environ Dev Sustain 8:271–287

[2] Rafatullah M, Ahmad T, Ghazali A et al (2013) Oil palm biomass as a precursor of activated carbons: a review. Crit Rev Env Sci Technol 43:1117–1161

[3] Ali GAM, Teo EYL, Aboelazm EAA et al (2017) Capacitive performance of cysteamine functionalized carbon nanotubes. Mater Chem Phys 197:100–104

[4] Zhang LL, Zhao X (2009) Carbon-based materials as supercapacitor electrodes. Chem Soc Rev 38:2520–2531

[5] Chang P-P, Wang C-Y, Kinumoto T et al (2018) Frame-filling C/C composite for high-performance EDLCs with high withstanding voltage. Carbon 131:184–192
[6] Kong L-B, Zhang J, An J-J et al (2008) MWNTs/PANI composite materials prepared by in situ chemical oxidative polymerization for supercapacitor electrode. J Mater Sci 43:3664–3669. https://doi.org/10.1007/s10853-008-2586-1
[7] Ali GAM, Manaf SAA, Kumar A et al (2014) High performance supercapacitor using catalysis free porous carbon nanoparticles. J Phys D Appl Phys 47:495307–495313
[8] Zhang J, Gong L, Sun K et al (2012) Preparation of activated carbon from waste Camellia oleifera shell for supercapacitor application. J Solid State Electrochem 16:2179–2186
[9] Chen X, Kierzek K, Jiang Z et al (2011) Synthesis, growth mechanism, and electrochemical properties of hollow mesoporous carbon spheres with controlled diameter. J Phys Chem C 115:17717–17724
[10] Okajima K, Ikeda A, Kamoshita K et al (2005) High rate performance of highly dispersed C60 on activated carbon capacitor. Electrochim Acta 51:972–977
[11] Borgohain R, Li J, Selegue JP et al (2012) Electrochemical study of functionalized carbon nano-onions for high-performance supercapacitor electrodes. J Phys Chem C 116:15068–15075
[12] Marina PE, Ali GAM, See LM et al (2016) In situ growth of redox-active iron-centered nanoparticles on graphene sheets for specific capacitance enhancement. Arab J Chem. https://doi.org/10.1016/j.arabjc.2016.1002.1006
[13] Zhou W, Zhou K, Liu X et al (2014) Flexible wire-like all-carbon supercapacitors based on porous core-shell carbon fibers. J Mater Chem A 2:7250–7255
[14] Hu W, Xie F, Li Y et al (2017) Hierarchically porous carbon derived from PolyHIPE for supercapacitor and deionization applications. Langmuir 33:13364–13375
[15] Chen A, Yu Y, Xing T et al (2015) Synthesis of graphitic carbon spheres for enhanced supercapacitor performance. J Mater Sci 50:5578–5582. https://doi.org/10.1007/s10853-015-9106-x
[16] Rufford TE, Hulicova-Jurcakova D, Khosla K et al (2010) Microstructure and electrochemical double-layer capacitance of carbon electrodes prepared by zinc chloride activation of sugar cane bagasse. J Power Sources 195:912–918
[17] Subramanian V, Luo C, Stephan AM et al (2007) Supercapacitors from activated carbon derived from banana fibers. J Phys Chem C 111:7527–7531
[18] Hegde G, Abdul Manaf SA, Kumar A et al (2015) Biowaste sago bark based catalyst free carbon nanospheres: waste to wealth approach. ACS Sustain Chem Eng 5:2247–2253
[19] Ali GAM, Divyashree A, Supriya S et al (2017) Carbon nanospheres derived from Lablab purpureus for high performance supercapacitor electrodes: a green approach. Dalton Trans 46:14034–14044
[20] Hernández-Montoya V, Ramírez-Montoya LA, Bonilla-Petriciolet A et al (2012) Optimizing the removal of fluoride from water using new carbons obtained by modification of nut shell with a calcium solution from egg shell. Biochem Eng J 62:1–7
[21] Habeeb OA, Ramesh K, Ali GAM et al (2017) Experimental design technique on removal of hydrogen sulfide using CaO-eggshells dispersed onto palm kernel shell activated carbon: experiment, optimization, equilibrium and kinetic studies. J Wuhan Univ Technol Mater Sci Ed 32:305–320
[22] Przepiórski J, Czyżewski A, Pietrzak R et al (2013) MgO/CaO-loaded porous carbons for carbon dioxide capture. J Therm Anal Calorim 111:357–364
[23] Ali GAM, Wahba OAG, Hassan AM et al (2015) Calcium-based nanosized mixed metal oxides for supercapacitor application. Ceram Int 41:8230–8234
[24] Habeeb OA, Ramesh K, Ali GAM et al (2017) Low-cost and eco-friendly activated carbon from modifed palm kernel shell for hydrogen sulfde removal from wastewater: adsorption and kinetic studies. Desalin Water Treat 84:205–214
[25] Lota K, Sierczynska A, Lota G (2011) Supercapacitors based on nickel oxide/carbon materials composites. Int J Electrochem 2011:1–6
[26] Ardizzone S, Fregonara G, Trasatti S (1990) "Inner" and "outer" active surface of RuO_2 electrodes. Electrochim Acta 35:263–267
[27] Ali GAM, Yusoff MM, Algarni H et al (2018) One-step electrosynthesis of MnO_2/rGO nanocomposite and its enhanced electrochemical performance. Ceram Int 44:7799–7807
[28] Zhi J, Wang Y, Deng S et al (2014) Study on the relation between pore size and supercapacitance in mesoporous carbon electrodes with silica-supported carbon nanomembranes. RSC Adv 4:40296–40300
[29] Kondrat S, Pérez CR, Presser V et al (2012) Effect of pore size and its dispersity on the energy storage in nanoporous supercapacitors. Energy Environ Sci 5:6474–6479
[30] Ali GAM, Yusoff MM, Shaaban ER et al (2017) High performance MnO_2 nanoflower supercapacitor electrode by electrochemical recycling of spent batteries. Ceram Int 43:8440–8448
[31] Borenstien A, Noked M, Okashy S et al (2013) Composite carbon nano-tubes (CNT)/activated carbon electrodes for non-aqueous super capacitors using organic electrolyte solutions. J Electrochem Soc 160:1282–1285
[32] Ma J, Xue T, Qin X (2014) Sugar-derived carbon/graphene composite materials as electrodes for supercapacitors. Electrochim Acta 115:566–572

[33] Selvakumar M, Krishna Bhat D (2008) Activated carbon-polyethylenedioxythiophene composite electrodes for symmetrical supercapacitors. J Appl Polym Sci 107:2165–2170

[34] Zheng J, Xiaomin R, Chuanli Q et al (2011) Hybrid supercapacitors based on polyaniline and activated carbon composite electrode materials. Pigm Res Technol 40:235–239

[35] Olad A, Gharekhani H (2015) Preparation and electrochemical investigation of the polyaniline/activated carbon nanocomposite for supercapacitor applications. Prog Org Coat 81:19–26

[36] Kujundziski AP, Chamovska D, Cvetkovska M et al (2012) Electrochemical study of electroconducting composite material–polypyrrole/activated carbon. Int J Electrochem Sci 7:4099–4113

[37] Zhang X, Sun X, Zhang H et al (2012) Development of redox deposition of birnessite-type MnO_2 on activated carbon as high-performance electrode for hybrid supercapacitors. Mater Chem Phys 137:290–296

[38] Yuan A, Zhang Q (2006) A novel hybrid manganese dioxide/activated carbon supercapacitor using lithium hydroxide electrolyte. Electrochem Commun 8:1173–1178

[39] Zhang L, Candelaria SL, Tian J et al (2013) Copper nanocrystal modified activated carbon for supercapacitors with enhanced volumetric energy and power density. J Power Sources 236:215–223

[40] Ni J, Yang L, Wang H et al (2012) A high-performance hybrid supercapacitor with $Li_4Ti_5O_{12}$–C nano-composite prepared by in situ and ex situ carbon modification. J Solid State Electrochem 16:2791–2796

[41] Selvakumar M, Bhat DK (2012) Microwave synthesized nanostructured TiO_2-activated carbon composite electrodes for supercapacitor. Appl Surf Sci 263:236–241

[42] Selvakumar M, Krishna Bhat D, Manish Aggarwal A et al (2010) Nano ZnO-activated carbon composite electrodes for supercapacitors. Phys B 405:2286–2289

[43] Kim CH, Kim B-H (2015) Zinc oxide/activated carbon nanofiber composites for high-performance supercapacitor electrodes. J Power Sources 274:512–520

[44] Tao T, Chen Q, Hu H et al (2012) MoO_3 nanoparticles distributed uniformly in carbon matrix for supercapacitor applications. Mater Lett 66:102–105

[45] Yuan G-H, Jiang Z-H, Aramata A et al (2005) Electrochemical behavior of activated-carbon capacitor material loaded with nickel oxide. Carbon 43:2913–2917

[46] Wang H-Q, Li Z-S, Huang Y-G et al (2010) A novel hybrid supercapacitor based on spherical activated carbon and spherical MnO_2 in a non-aqueous electrolyte. J Mater Chem 20:3883–3889

[47] Li Y, Kang L, Bai G et al (2014) Solvothermal synthesis of Fe_2O_3 loaded activated carbon as electrode materials for high-performance electrochemical capacitors. Electrochim Acta 134:67–75

[48] Lin C, Ritter JA, Popov BN (1999) Development of carbon-metal oxide supercapacitors from sol-gel derived carbon-ruthenium xerogels. J Electrochem Soc 146:3155–3160

[49] Kim M, Hwang Y, Min K et al (2013) Introduction of MnO_2 nanoneedles to activated carbon to fabricate high-performance electrodes as electrochemical supercapacitors. Electrochim Acta 113:322–331

[50] Zhang D, Zhang X, Chen Y et al (2012) An environment-friendly route to synthesize reduced graphene oxide as a supercapacitor electrode material. Electrochim Acta 69:364–370

[51] Aboutalebi SH, Salari M, Konstantinov K et al (2011) Comparison of GO, GO–MWCNTs composite. Energy Environ Sci 4:1855–1865

[52] Ali GAM, Makhlouf SA, Yusoff MM et al (2015) Structural and electrochemical characteristics of graphene nanosheets as supercapacitor electrodes. Rev Adv Mater Sci 41:35–43

[53] Ali GAM, Manaf SAA, Divyashree A et al (2016) Superior supercapacitive performance in porous nanocarbons. J Energy Chem 25:734–739

[54] Farma R, Deraman M, Awitdrus A et al (2013) Preparation of highly porous binderless activated carbon electrodes from fibres of oil palm empty fruit bunches for application in supercapacitors. Bioresour Technol 132:254–261